ISSUE: May 2025

How Active EMI Filter ICs Reduce Common-Mode Emissions in Single- And Three-Phase Applications (Part 5): Improving Immunity To Low-Frequency Disturbances

by Timothy Hegarty, Texas Instruments, Phoenix, Ariz.

A compact design of the electromagnetic interference (EMI) filter is vital to meeting packaging specifications in high-density ac-dc applications, such as server-rack ac-dc power supplies for enterprise and onboard chargers (OBCs) for automotive applications. Fortunately, an active EMI filter (AEF) circuit for common-mode (CM) noise attenuation, through miniaturization of the toroidal-cored CM chokes in the equivalent passive filter, can considerably reduce the size, weight and cost of the overall power-circuit implementation.

Part 1 of this article series [1] provided an overview of AEF techniques to diminish the reliance on bulky passive filter components. Parts 2 and 3 discussed behavioral models to suitably characterize the impedance of ferrite [2] and nanocrystalline [3] chokes, respectively. Part 4 examined small-signal stability[4] by deriving loop-gain expressions for a feedback-type voltage-sense current-inject (FB-VSCI) AEF circuit, implemented using an integrated circuit (IC), TI's TPSF12C3-Q1.

However, the frequency response of an AEF circuit below 150 kHz can result in large-signal voltage saturation at the output of the AEF amplifier when low-frequency CM conducted disturbances exist at the filter's input port. To this end, this fifth installment of the series examines a multiple feedback (MFB) technique to improve the immunity behavior below 150 kHz while preserving the filter attenuation performance for high-frequency emissions above 150 kHz. This article summarizes the challenges related to CM low-frequency conducted disturbances, analyzes the proposed MFB circuit modification, and concludes with simulations and experimental validation of a single-phase AEF circuit with MFB.

Active Filtering—Why It's Needed And The Low-Frequency Issue

Higher power levels and the increased number of fast-switching power semiconductor devices in space-limited power-conversion systems result in a more challenging electromagnetic environment with additional EMI sources and victims present in end equipment. Some examples are telecommunications rectifiers, server-rack power supplies and automotive OBCs. To this end, the topic of active filtering[1-9] has garnered significant attention in power electronics-constrained applications, owing to the associated improvements in power density and cost relative to traditional passive filter designs.

A cost-effective and high-density filter is a challenge in switching regulator implementations. Yet it is essential to effectively package the complete solution within demanding chassis-enclosed form factors. Given touch-current safety requirements, CM EMI filters for grid-tied applications often have limited Y-capacitance values and thus require large-sized CM chokes to achieve a target corner frequency or filter attenuation. This can give rise to unsatisfactory passive filter designs with bulky and expensive CM chokes that impact the overall filter size.

Fortunately, in both single- and three-phase high-density power electronics applications, commercially available active power-supply filter ICs reduce magnetic component and filter size by amplifying the effective Y-capacitance value[6] over a prescribed frequency range. This reduction helps comply with applicable conducted emissions standards while increasing the volumetric and gravimetric power densities of the overall implementation.

However, low-frequency disturbances can adversely impact the linear operation of AEF circuits. This is especially true as the AEF response is optimized for noise attenuation in the frequency band for EMI measurements (150 kHz to 30 MHz for CISPR 11 and CISPR 32). Low-frequency oscillations or disturbances, typically less than 100 kHz, exist in systems arising from factors such as low switching frequency and topology-related nonlinear behavior,[10] as well as grid-side low-frequency disturbances.

© 2025 How2Power. All rights reserved.

Passive filter components provide less attenuation at low frequencies, leading the AEF circuit to sense a higher noise amplitude. When multiplied by the AEF gain, the amplifier[6-7] output voltage can saturate low or high, thus impacting overall EMI filter performance.

Gain profile shaping of a CM AEF circuit with an MFB network can improve CM rejection below 150 kHz, thus boosting the immunity to low-frequency conducted disturbances while preserving noise attenuation performance above 150 kHz.

AEF Review

FB-VSCI AEF Circuit

Fig. 1 shows the schematics for a two-stage passive-only filter and an equivalent active filter design. The single-phase AEF solution uses an FB-VSCI topology[2] and is scalable to three-phase systems with or without a neutral connection. The method provides a high level of integration by virtue of an IC approach and maintains high density by avoiding magnetic components for sensing and injection. Positioned between the CM chokes designated L_{CM1} and L_{CM2} in Fig. 1, the AEF circuit for this single-phase application provides a lower-impedance shunt path for CM noise currents to flow to chassis ground.

The design targets a reduction of the filter volume, yet maintains low values of the low-frequency earth leakage current using an active circuit that shapes the frequency response of the inject capacitor—effectively multiplying its value at high frequencies.[1] In turn, this amplified inject capacitance over the required frequency range is the key to achieving lower CM choke inductances relative to the values of a passive filter with a comparable attenuation profile.

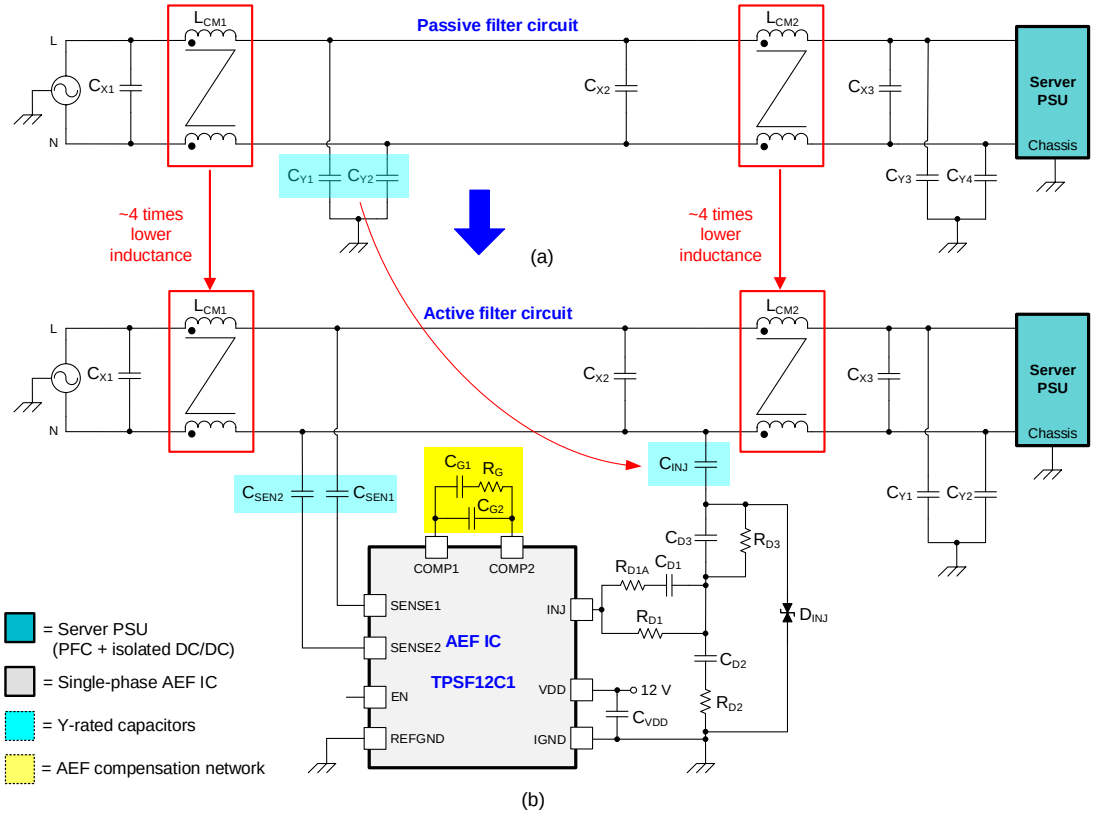

Fig. 1. Schematic of a passive filter (a) replaced by a corresponding AEF circuit (b).

The AEF design in Fig. 1b leverages high-voltage Y-rated capacitors, highlighted in cyan, in combination with low-voltage active circuits within the IC for sensing and injection. The output of the power amplifier (at the INJ pin) injects the required noise-cancelling signal back into the power lines through a damping network and a Y-

© 2025 How2Power. All rights reserved.

rated inject capacitor C_{INJ}., and an X-capacitor C_{X2}, which is positioned between the CM chokes. This effectively provides a low-impedance path between the power lines from a CM noise standpoint, up to low megahertz frequencies.

This technique allows current injection directly onto one power line using just one inject capacitor. Inclusion of the damping network shapes the amplifier-output-to-inject-capacitor transfer function to stabilize the LC resonant behavior that occurs between the CM choke inductances and the inject capacitance. Up to 25 dB of CM noise attenuation is possible with this AEF circuit in the frequency range from 150 kHz to 3 MHz.[2-5]

The AEF IC (Texas Instruments' TPSF12C1[11]) for this single-phase application, positioned between the CM chokes designated as L_{CM1} and L_{CM2} in Fig. 1, provides a lower-impedance shunt path for CM currents to flow to chassis ground. The active circuit shapes the frequency response of the inject capacitor, effectively multiplying its value at high frequencies. In turn, this amplified inject capacitance over the required frequency range lowers CM choke inductances relative to the values of a passive filter with equivalent attenuation.

AEF With Conventional Feedback

As illustrated in Fig. 2, the AEF circuit rejects the line-frequency ac voltage using a two-stage high-pass filter (HPF) sensing network, while amplifying the detected high-frequency CM noise and maintaining closed-loop stability using an external tunable damping circuit with impedance branches indicated as Z_{D1}, Z_{D2} and Z_{D3} (see also the components with subscript "D" reference designators in Fig. 2).

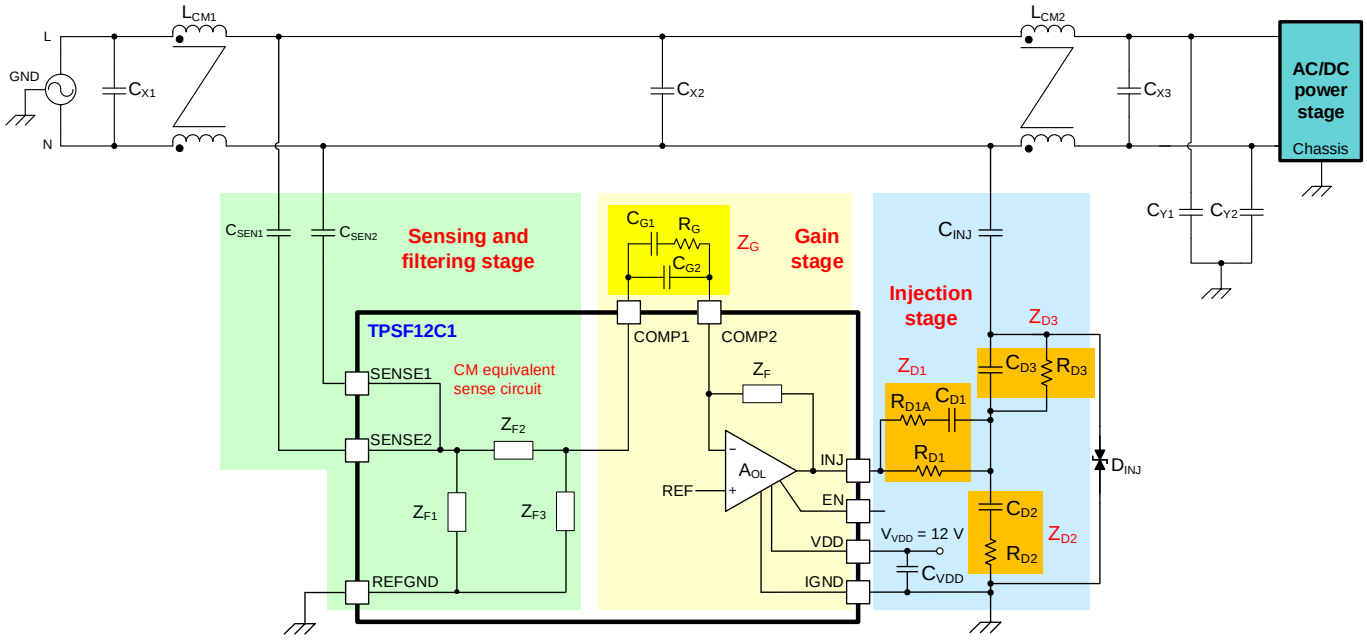

Fig. 2. CM-equivalent functional block diagram of the single-phase FB-VSCI AEF IC with conventional feedback.

The CM disturbance voltage is sensed by sense capacitors C_{SEN1} and C_{SEN2} and goes through both the HPF network and a CM-noise summation network.[4] Impedance Z_G (with external components designated R_G, C_{G1} and C_{G2}) connected between the COMP1 and COMP2 pins sets the AEF amplification gain characteristic, along with an integrated feedback impedance denoted as Z_F.

The amplifier in Fig. 2 establishes the closed-loop (CL) gain, which is the transfer function from the sensed and filtered CM disturbance at the COMP1 pin to the amplifier output at the INJ pin. Equation 1 expresses this CL gain as

© 2025 How2Power. All rights reserved.

$$A_{CL}(s) = -\frac{Z_F(s)}{Z_G(s)} \cdot \frac{1}{1+\frac{1+Z_F(s)/Z_G(s)}{A_{OL}(s)}} \quad (1)$$

where $A_{OL}(s)$ is the open-loop (OL) amplifier gain.

The AEF gain from LINE to INJ is then the product of the sensing gain $A_{SENSE}(s)$ from LINE to COMP1 and the CL gain $A_{CL}(s)$ from COMP1 to INJ. The AEF gain is important, as it determines the impedance reduction (or capacitance boosting effect) of the inject capacitor by the AEF circuit, as expressed by equation 2:

$$Z_{AEF}(s) = \frac{Z_{Cinj}(s)}{1-G_{AEF}(s)} \quad (2)$$

Equation 3 calculates the AEF gain as:

$$G_{AEF}(s) = A_{SENSE}(s)A_{CL}(s) \quad (3)$$

Sub-150-kHz CM Conducted Disturbances

General

CM conducted disturbances at frequencies less than 150 kHz may influence the reliable operation of equipment installed in residential, commercial and automotive environments. Such disturbances may emanate from the power distribution grid, from adjacent power electronics equipment, or from the equipment itself during nonlinear operating intervals. The disturbances from the grid may exist at the fundamental line frequency as well as its harmonics and interharmonics. Meanwhile, power electronic converters and motor drives can inject CM disturbances into the ground conductors and earthing system through capacitive coupling.

IEC 61000-4-6 is the applicable standard[12] to evaluate functional immunity performance when equipment is subject to low-frequency CM-conducted disturbances. Specified test levels range from 15 Hz to 150 kHz, with amplitudes classified from level 1 to level 4 (practical conditions range mainly between levels 2 and 3, approximately 1 Vrms to 10 Vrms).

Impact Of Low-Frequency Disturbances On AEF

The schematic in Fig. 2 shows an AEF circuit with a conventional feedback compensation technique; compensation components (shaded in yellow) connect from pins designated COMP1 and COMP2. Optimizing the AEF noise sensing, processing and amplification circuits typically offers high AEF gain, corresponding to maximum attenuation performance, for emissions in the EMI measurement frequency band. Generic standards such as CISPR 11 and CISPR 32, along with product family standards such as IEC 61851-21-1 for OBCs,[13] specify limits for conducted emissions starting at 150 kHz.

However, CM disturbances under 150 kHz can significantly impact the operation of the AEF circuit. In addition to the grid-side transients and capacitive coupling effects mentioned in the previous section, low-frequency disturbances can originate from other factors, such as:

- The switching-frequency ripple of the power factor correction (PFC) stage, with typical frequencies ranging from 45 kHz to 70 kHz.
- Topology-related nonideal switching, such as undesirable current spikes that occur near the zero-voltage crossings of the ac mains voltage with a totem-pole (TTPL) PFC[10] when the line-frequency leg changes state.
- Resonant disturbances when disabling switching around the input-voltage zero crossings for efficiency optimization.

© 2025 How2Power. All rights reserved.

Moreover, the CM choke and Y-capacitor passive components offer little passive attenuation at low frequencies, meaning that the sensed noise amplitude on the power lines between the CM chokes (L_{CM1} and L_{CM2} in Fig. 1b) is relatively high.

With a large line-voltage-sensed noise amplitude multiplied by the AEF gain, the adverse outcome is voltage saturation at the AEF amplifier output for a given dynamic range. The swing is limited by the supply voltage of the amplifier, typically 12 V. This compromises EMI filtering during at least part of the mains cycle and thus degrades AEF performance relative to a passive EMI filter. In ac-dc systems there exists a clear need to improve the low-frequency rejection of CM disturbances while keeping the high-frequency gain performance intact.

MFB Approach

Block Diagram

Fig. 3 shows the proposed MFB arrangement for an AEF to increase the rejection of low-frequency disturbances. Aside from the addition of three impedance blocks denoted with "MFB"-suffixed designators, the circuit shown is similar to Fig. 2. The MFB approach offers frequency-dependent gain shaping to enhance the rejection of CM disturbances below 150 kHz while maintaining AEF performance and loop stability[4] above 150 kHz.

The MFB compensation network components connect between the COMP1, COMP2 and INJ nodes, as highlighted in yellow in Fig. 3. The supplementary network balances the necessary low-frequency attenuation while maximizing the high-frequency gain.

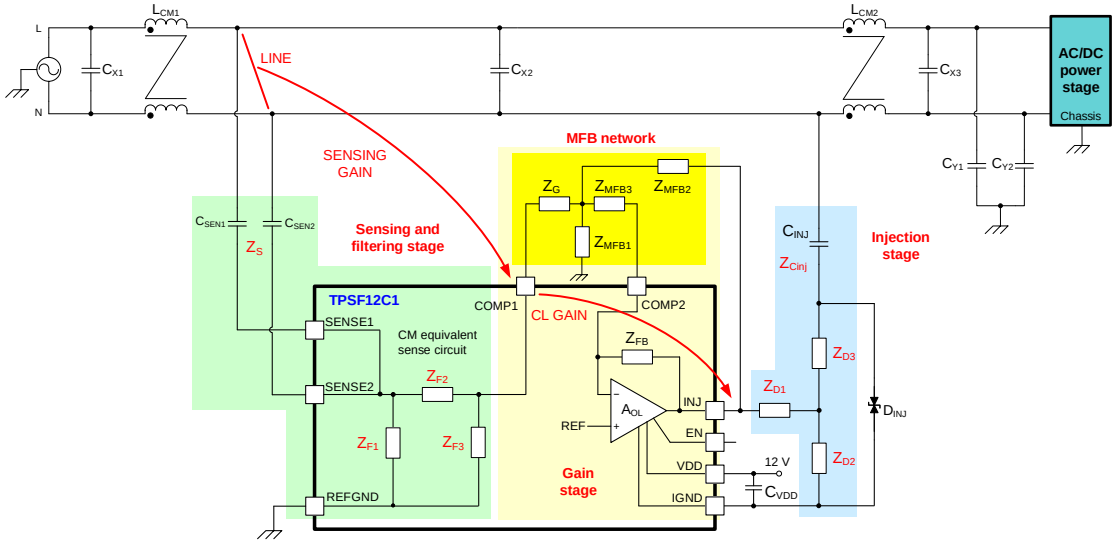

Fig. 3. CM-equivalent block diagram of the single-phase FB-VSCI AEF circuit with MFB.

As shown in Fig. 4, MFB components designated R_{MFB1}, R_{MFB2}, C_{MFB1}, C_{MFB2} and C_{MFB3}, along with original compensation components R_G, C_{G1} and C_{G2}, create a second-order HPF in the feedback network. More specifically, components C_{G2} and C_{MFB2} set the high-frequency gain, while R_G and C_{MFB1} tune the phase margin of the loop-gain characteristic.

© 2025 How2Power. All rights reserved.

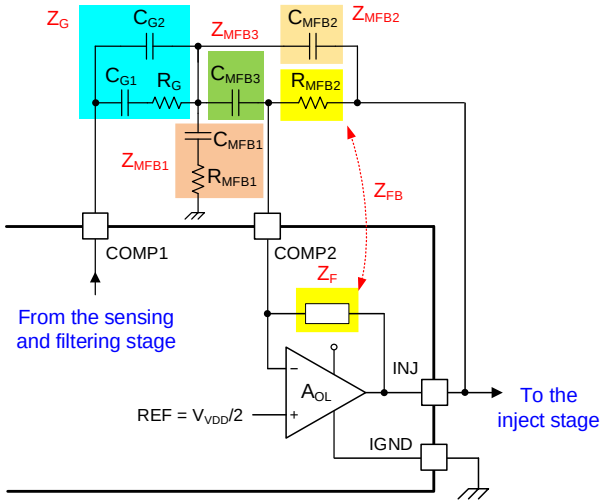

Fig. 4. AEF amplifier and MFB components.

Amplifier Gain Stage Model

Fig. 5 illustrates a generalized CM circuit model including the amplifier and relevant impedance blocks within the sensing and gain stages.

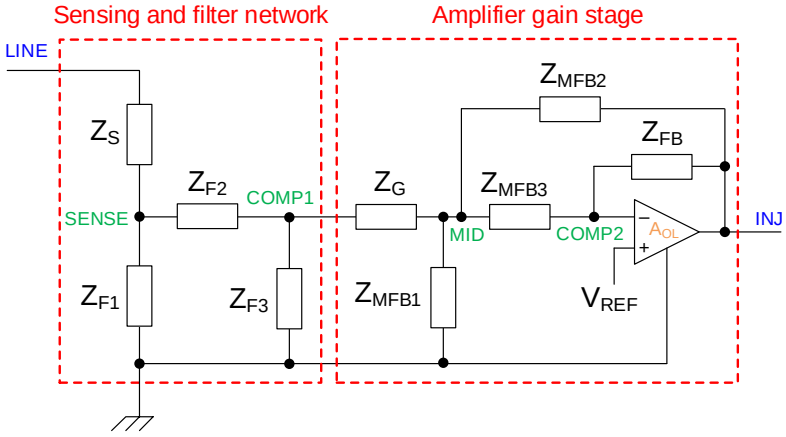

Fig. 5. Sensing, filtering and amplification circuit model with MFB.

Z_S in Fig. 5 is the effective CM impedance of the sense capacitor network, which is part of the second-order HPF along with impedances designated Z_{F1}, Z_{F2} and Z_{F3} internal to the IC. Meanwhile, Z_{FB}, Z_G and $Z_{MFB1\text{-}3}$ denote the impedances pertinent to the amplifier gain stage. Referring to Fig. 4, equation 4 shows that these impedances are

© 2025 How2Power. All rights reserved.

$$Z_{FB}(s) = Z_F(s) \| R_{MFB2}$$
$$Z_G(s) = \left(R_G + \frac{1}{sC_{G1}} \right) \Bigg\| \frac{1}{sC_{G2}}$$
$$Z_{MFB1}(s) = R_{MFB1} + \frac{1}{sC_{MFB1}} \quad (4)$$
$$Z_{MFB2}(s) = \frac{1}{sC_{MFB2}}$$
$$Z_{MFB3}(s) = \frac{1}{sC_{MFB3}}$$

AEF Gain Derivation

The derivation of expressions for AEF gain builds on previously presented analysis[4] but with revised feedback impedances around the AEF amplifier, denoted as Z_{MFB1-3} in Fig. 3. Equation 5 expresses the sensing gain from LINE to COMP1 as:

$$A_{SENSE}(s) = \frac{V_{COMP1}(s)}{V_{LINE}(s)} = \frac{Z_{F1} \| (Z_{F2} + Z_{F3})}{Z_S + Z_{F1} \| (Z_{F2} + Z_{F3})} \cdot \frac{Z_{F3}}{Z_{F2} + Z_{F3}} \quad (5)$$

The amplifier model in Fig. 5 establishes the CL gain, which is effectively the transfer function from the sensed and filtered CM disturbance at the COMP1 pin to the amplifier output at the INJ pin. Equating the currents around the amplifier using Kirchhoff's law while neglecting the effect of the finite amplifier OL gain results in equations 6 and 7:

$$\frac{V_{COMP1} - V_{MID}}{Z_G} = \frac{V_{MID}}{Z_{MFB1}} + \frac{V_{MID} - V_{INJ}}{Z_{MFB2}} + \frac{V_{MID}}{Z_{MFB3}} \quad (6)$$

$$\frac{V_{MID}}{Z_{MFB3}} = -\frac{V_{INJ}}{Z_{FB}} \quad (7)$$

Eliminating V_{MID} and solving for the CL gain results in equation 8:

$$A_{CL\text{-}MFB}(s) = \frac{V_{INJ}(s)}{V_{COMP1}(s)} = -\frac{Z_{FB}}{Z_G} \cdot \frac{1}{1 + \frac{Z_{MFB3}}{Z_G \| Z_{MFB1} \| Z_{MFB2}} + \frac{Z_{FB}}{Z_{MFB2}}} \quad (8)$$

Clearly, equation 8 bears similarity to equation 1 for conventional feedback but with a factor denoted in blue to adjust for MFB. As Fig. 3 indicates, the AEF gain, $G_{AEF}(s)$, is the product of the sensing gain and CL gain given by equation 5 and equation 8, respectively.

Analytical Results

Based on the derived expressions above, Fig. 6 shows the AEF gain for conventional and MFB implementations in a typical single-phase design.[8] As shown, the MFB network provides an additional 23 dB of rejection for CM disturbances at 30 kHz.

© 2025 How2Power. All rights reserved.

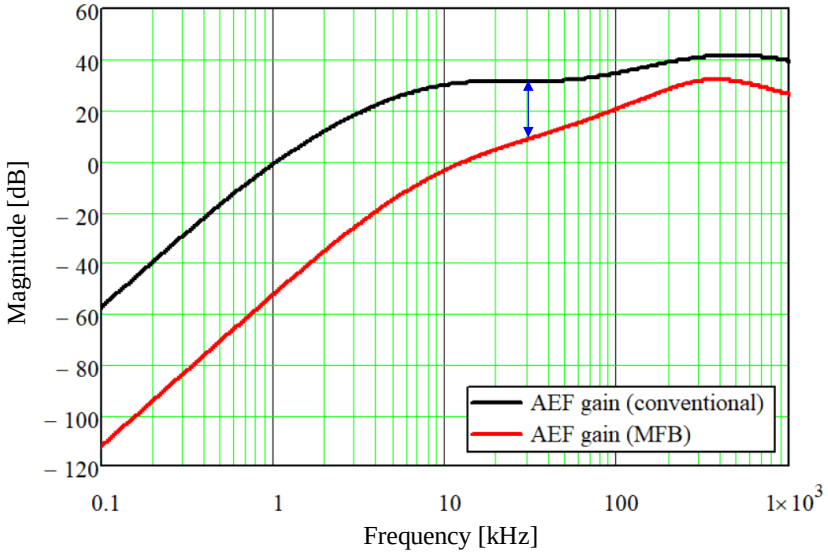

Fig. 6. Analytically derived AEF gain plot using the conventional feedback and MFB networks.

Simulation And Experimental Results

Simulation Results

Fig. 7 is a SIMPLIS simulation result using the same single-phase filter design as that used for the analytical results. The simulated AEF gain from LINE to INJ for the conventional and MFB approaches demonstrates close agreement with the calculated plot of Fig. 6, thus confirming the validity of the analytical approach.

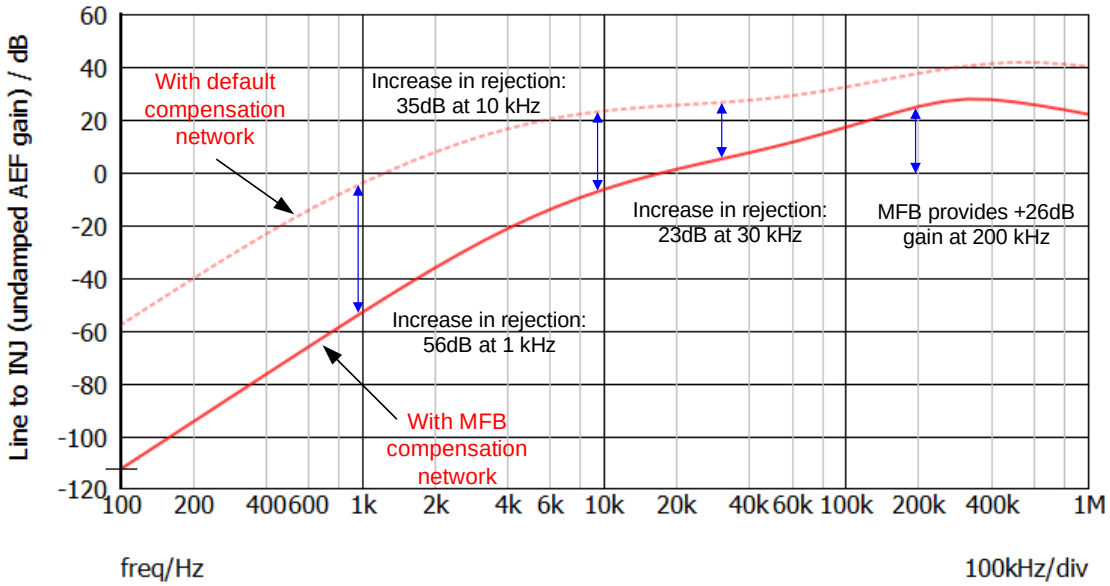

Fig. 7. Simulated AEF gain with conventional and MFB compensation networks.

Fig. 8 is a simulation result of the INJ voltage swing with and without MFB while applying a sinusoidal CM disturbance of 3 V at 30 kHz at the input port of the EMI filter (that is, from the neutral terminal to chassis ground).

© 2025 How2Power. All rights reserved.

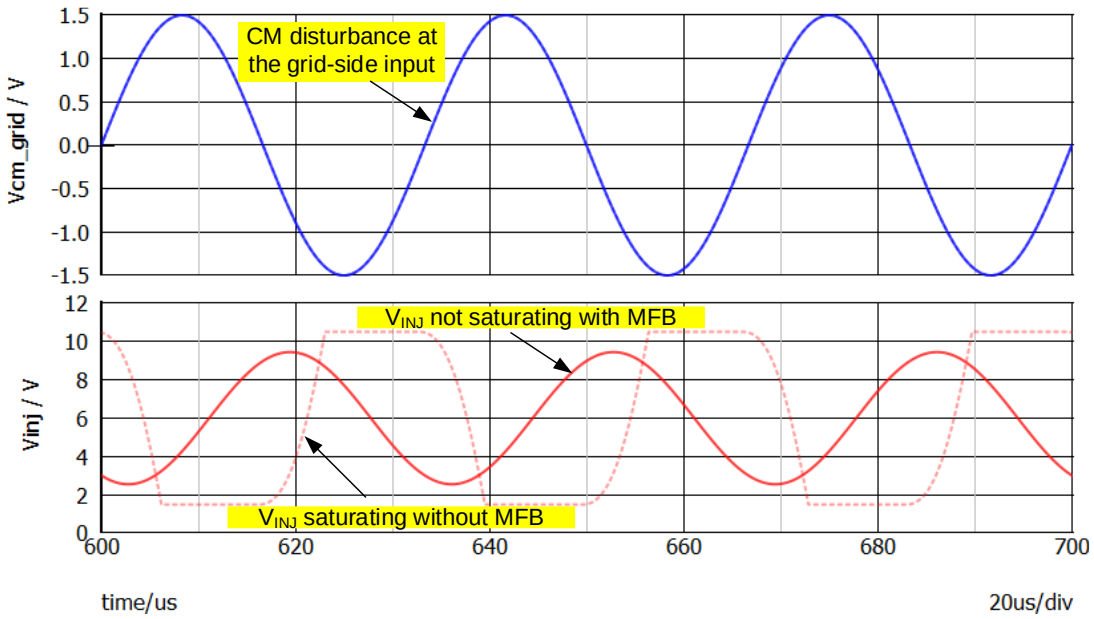

Fig. 8. Simulated INJ voltage with a CM voltage of 3 Vpp at 30-kHz applied at the filter input.

Practical Results

Fig. 9 shows a single-phase evaluation board[8] for an AEF rated at 10 Arms. The nanocrystalline-cored CM chokes[3] from Würth Elektronik each have a rated inductance of 2 mH. The Y-capacitors connected from the live and neutral lines to chassis ground at the input (grid side) and output (regulator side) of the filter are each 2.2 nF. The inject capacitor is 4.7 nF.

Fig. 9. Single-phase AEF circuit with MFB.

The measured INJ voltage waveform in Fig. 10 occurs when injecting a sine-wave CM disturbance of 3 Vpp at 30 kHz at the input side of the filter. The MFB circuit maintains linear operation, matching the simulated result in Fig. 8.

© 2025 How2Power. All rights reserved.

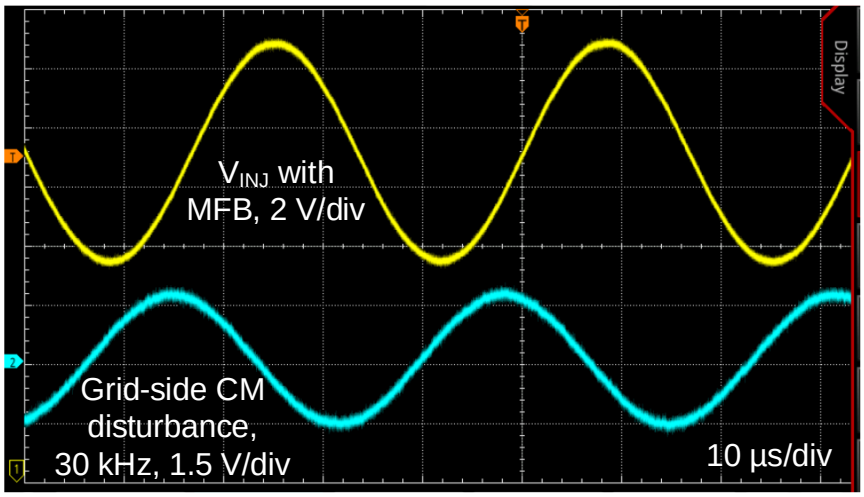

Fig. 10. Time-domain measurements while injecting a CM disturbance with the default circuit indicating saturation (a), and the MFB circuit operating linearly (b).

The AEF gain at 30 kHz went from approximately 31 dB to 8 dB with MFB, thus helping maintain linear operation and avoid saturation. Another circuit improvement is to increase the AEF IC supply voltage (see V_{VDD} in Fig. 2) from 12 V to 24 V, which biases INJ at a higher voltage and thus further expands the available dynamic range.

Summary

AEF circuits now receive significant attention for power electronics-constrained applications, owing to the attendant improvements in power density and cost of the EMI filter. Gain profile shaping of a CM AEF circuit with a supplementary MFB network to increase the CM rejection in the sub-150-kHz range avoids voltage saturation at the amplifier output caused by low-frequency CM-conducted disturbances in the system. Close agreement of the formulated analytical results with simulation modeling and experimental measurements substantiates the theoretical approach described.

References

1. "How Active EMI Filter ICs Reduce Common-Mode Emissions In Single- And Three-Phase Applications (Part 1): An Overview" by Timothy Hegarty, How2Power Today, November 2023 issue.

2. "How Active EMI Filter ICs Reduce Common-Mode Emissions In Single- And Three-Phase Applications (Part 2): Modeling Ferrite Chokes" by Timothy Hegarty, How2Power Today, February 2024 issue.

3. "How Active EMI Filter ICs Reduce Common-Mode Emissions In Single- And Three-Phase Applications (Part 3): Modeling Nanocrystalline Chokes" by Timothy Hegarty, How2Power Today, March 2024 issue.

4. "How Active EMI Filter ICs Reduce Common-Mode Emissions In Single- And Three-Phase Applications (Part 4): Loop-Gain Analysis" by Timothy Hegarty, How2Power Today, June 2024 issue.

5. "Experimental and Simulation Based Analysis of an Active EMI Filter for Automotive PFC Applications," by Patrick Körner et al., 2024 Energy Conversion Congress and Expo (ECCE Europe), Germany, September 2024, pp. 1-7.

6. "A Critical Analysis of Amplifier Requirements in Capacitance-Boosting Circuits for EMI Reduction," by Markeljan Fishta et al., 2024 14th International Workshop on the Electromagnetic Compatibility of Integrated Circuits (EMC Compo), Torino, Italy, October 2024, pp. 1-5.

© 2025 How2Power. All rights reserved.

7. "Multiple Feedback Architecture to Improve the Low-Frequency Immunity of an Active EMI Filter" by Timothy Hegarty, Naresh Adepu and Abhijeet Godbole, PCIM Europe 2025; Nuremberg, Germany, May 2025.

8. "TPSF12C1EVM-FILTER active EMI filter evaluation module for single-phase AC power systems," Texas Instruments, July 2023.

9. "TPSF12C1 and TPSF12C3 power-supply filter IC FAQs," TI E2E design support forums, August 2023.

10. "How to reduce current spikes at AC zero-crossing for totem-pole PFC," by Bosheng Sun, TI Analog Applications Journal, November 2015.

11. TPSF12C1 product page, Texas Instruments website.

12. Testing and measurement techniques – Test for immunity to conducted, common-mode disturbances in the frequency range 0 Hz to 150 kHz," IEC 61000-4-16, second edition, December 2015.

13. "Electric vehicle conductive charging system – Part 21-1 Electric vehicle on-board charger EMC requirements for conductive connection to AC/DC supply," IEC 61851-21-1, first edition, June 2017.

About The Author

Timothy Hegarty is a senior member technical staff in the Switching Regulators business unit at Texas Instruments. With over 25 years of power-management engineering experience, he has written numerous conference papers, technical articles, seminars, white papers and application notes. Tim's current focus is on enabling technologies for high-frequency, low-EMI, isolated and nonisolated switching regulators with a wide input-voltage range, targeting industrial, enterprise and automotive applications. He is a senior member of the IEEE and a member of the IEEE Power Electronics Society.

For more on EMI and electromagnetic compatibility topics in power-supply design, see How2Power's Power Supply EMI Anthology.

© 2025 How2Power. All rights reserved.